Three-dimensional Bayesian optical diffusion tomography with experimental data

Adam B. Milstein, Seungseok Oh, Jeffery S. Reynolds, Kevin J. Webb, and Charles A. Bouman

School of Electrical and Computer Engineering, Purdue University, West Lafayette, Indiana 47907-1285

Rick P. Millane

Department of Electrical and Computer Engineering, University of Canterbury, Private Bag 4800, Christchurch, New Zealand

Received July 20, 2001

Reconstructions of a three-dimensional absorber embedded in a scattering medium by use of frequency domain measurements of the transmitted light in a single source–detector plane are presented. The reconstruction algorithm uses Bayesian regularization and iterative coordinate descent optimization, and it incorporates estimation of the detector noise level, the source–detector coupling coefficient, and the background diffusion coefficient in addition to the absorption image. The use of multiple modulation frequencies is also investigated. The results demonstrate the utility of this algorithm, the importance of a three-dimensional model, and that out-of-plane scattering permits recovery of three-dimensional features from measurements in a single plane.

OCIS codes: 100.3010, 100.3190, 100.6890, 170.5280.

Quantitative imaging of soft tissue by use of light offers chemical specificity through spectroscopy, and instruments can be safe and inexpensive.[1] Thus there is increasing interest in optical diffusion imaging, for which the spatially dependent scatter and absorption are to be reconstructed by use of measured data with a number of source and detector locations and a diffusion equation forward model.[2] However, for *in vivo* optical imaging to become practical, accurate three-dimensional (3-D) imaging in the heavily scattering tissue environment is necessary. We previously reported accurate and efficient inversions for two-dimensional (2-D) test problems, using nonlinear optimization in a Bayesian framework.[3,4] Others have reported iterative approaches based on a 2-D diffusion equation forward model with experimental data.[5,6] Whereas the validity of a 2-D diffusion model for realistic problems has been investigated and corrections proposed, it is clear that, in general, accounting for out-of-plane scattering will require a 3-D solution.[7]

Here we extend our previous 2-D Bayesian[3] formulation and iterative coordinate descent optimization method for absorption imaging to three dimensions, and we address the problem of estimating source–detector coupling, the background diffusion coefficient, and detector noise variance, thereby circumventing the need for difficult and inconvenient calibration measurements of homogeneous phantoms. The estimation of source–detector coupling loss and background parameters by a preprocessing technique with an assumed homogeneous domain has been described,[6] and the source–detector coupling coefficients have been estimated as part of a linear generalized inverse.[8] Here we incorporate estimation of the ancillary parameters into the Bayesian framework and update the estimates throughout the inversion procedure. We use laboratory data to assess the algorithm and the merits of using multiple modulation frequencies.

The frequency domain diffusion equation[1] models the propagation of modulated light in a highly scattering medium. The complex modulation envelope of the photon flux $\phi_k(r)$ at position r that is due to a point source at position s_k satisfies

$$\nabla \cdot [D(r)\nabla\phi_k(r)] + [-\mu_a(r) - j\omega/c]\phi_k(r) = -\delta(r - s_k), \tag{1}$$

where c is the speed of light in the medium, ω is the modulation frequency, $D(r)$ is the diffusion coefficient, and $\mu_a(r)$ is the absorption coefficient. Extrapolated Dirichlet boundary conditions, which account for refractive-index mismatch, may be imposed to model absorbing boundaries.[9]

We consider the case of a spatially variable absorption coefficient and a constant (but unknown) diffusion coefficient. The set of absorption coefficients and the diffusion coefficient are denoted by vector $\mathbf{x}$, where $\mathbf{x} = [\mu_a(r_1), \ldots, \mu_a(r_N), D]^T$, and the domain of the scattering region is discretized into N points at positions r_i. The forward model is expressed as a complex vector $\mathbf{f}(\mathbf{x}) = [\mathbf{f}_{\omega_1}(\mathbf{x}), \mathbf{f}_{\omega_2}(\mathbf{x}), \ldots, \mathbf{f}_{\omega_Q}(\mathbf{x})]^T$, where $\mathbf{f}_{\omega_i}(\mathbf{x})$ is the computed data vector for $\omega = \omega_i$ that corresponds to all source and detector pairs. The true measurements that correspond to $\mathbf{f}(\mathbf{x})$ are collected into column vector $\mathbf{y}$ of length $P = KMQ$, where there are K source positions, M detector positions, and Q modulation frequencies. The solution of the optical imaging problem will determine image $\mathbf{x}$ from measurements $\mathbf{y}$.

Formulating the solution in a Bayesian framework,[3] we compute the maximum *a posteriori* estimate of $\mathbf{x}$ (the image) and simultaneously maximize the conditional density with respect to α (a parameter that scales detector noise variance) and γ (the source–detector coupling coefficient). More precisely, the maximum *a posteriori* estimate is given by

0146-9592/02/020095-03$15.00/0

$$\hat{\mathbf{x}} = \arg \max_{x \geq 0} \max_{\alpha} \max_{\gamma} [\log p(\mathbf{y}|\mathbf{x}, \alpha, \gamma) + \log p(\mathbf{x})], \tag{2}$$

where $p(\mathbf{y}|\mathbf{x}, \alpha, \gamma)$ is the data likelihood and $p(\mathbf{x})$ is the prior density for the image. The data likelihood is formed by use of a Gaussian model.[3] For the prior density, we use the generalized Gaussian Markov random field model[3]

$$p(\mathbf{x}) = \frac{1}{\sigma^N z(p)} \exp\left[-\frac{1}{p\sigma^p} \sum_{\{i,j\} \in \mathcal{N}} b_{i-j} |x_i - x_j|^p \right], \quad 1 \leq p \leq 2, \tag{3}$$

where σ and p are hyperparameters (where $p = 2$ corresponds to the Gaussian case), $\mathcal{N}$ consists of all pairs of neighboring nodes, and b_{i-j} represents coefficients in a 26-node neighborhood system with values inversely proportional to node separation.

We assume here that γ is real and is the same for all source–detector pairs, which is appropriate for our experimental arrangement. With α and γ unknown, and using the data and prior density functions, we can rewrite Eq. (2) as

$$\hat{\mathbf{x}} = \arg \min_{x \geq \mathbf{0}} \min_{\gamma} \min_{\alpha} \left[\frac{1}{\alpha} \|\mathbf{y} - \gamma \mathbf{f}(\mathbf{x})\|_{\Lambda}{}^2 + P \log \alpha + \frac{1}{p\sigma^p} \sum_{\{i,j\} \in \mathcal{N}} b_{i-j} |x_i - x_j|^p \right], \tag{4}$$

where Λ is the inverse of a diagonal covariance matrix and $\|\mathbf{w}\|_{\Lambda}{}^2 = \mathbf{w}^H \Lambda \mathbf{w}$. Viewing the argument in Eq. (4) as a cost function, we sequentially update α, γ, and $\mathbf{x}$ in an iterative optimization scheme. Minimization with respect to α, assuming that γ and $\mathbf{x}$ are constant, gives $\hat{\alpha} = P^{-1} \|\mathbf{y} - \hat{\gamma} \mathbf{f}(\hat{\mathbf{x}})\|_{\Lambda}{}^2$. Minimizing with respect to γ for constant α and $\mathbf{x}$ gives

$$\hat{\gamma} = \frac{\mathrm{Re}[\mathbf{f}^H(\hat{\mathbf{x}}) \Lambda \mathbf{y}]}{\mathbf{f}^H(\hat{\mathbf{x}}) \Lambda \mathbf{f}(\hat{\mathbf{x}})}, \tag{5}$$

where H denotes the conjugate transpose. The update with respect to D consists of one iteration of a one-dimensional Newton's method, with step

$$\Delta \hat{D} = \frac{\mathrm{Re}[\mathbf{e}^H \mathbf{f}_D{}'^H(\hat{\mathbf{x}}) \Lambda \mathbf{z}]}{\hat{\gamma} \mathbf{e}^H \mathbf{f}_D{}'^H(\hat{\mathbf{x}}) \Lambda \mathbf{f}_D{}'(\hat{\mathbf{x}}) \mathbf{e}}, \tag{6}$$

where $\mathbf{e} = [1, 1, \ldots, 1]^T$, $\mathbf{z} = \mathbf{y} - \hat{\gamma} \mathbf{f}(\hat{\mathbf{x}})$, and $\mathbf{f}_D{}'(\hat{\mathbf{x}})$ is the $P \times N$ Fréchet derivative[10] of $\mathbf{f}(\,)$ at $\hat{\mathbf{x}}$ with respect to D. The update of the μ_a components of $\mathbf{x}$ employs the iterative coordinate descent algorithm.[3]

Measurements were made of an optically clear culture flask containing a black plastic cylinder of 0.7-cm diameter embedded in a turbid suspension, as shown in Fig. 1. The region of the flask containing the suspension had dimensions 8.1 cm × 2.9 cm × 8.1 cm. The suspension was a phosphate-buffered saline solution of Intralipid diluted to a concentration of 0.4%. The data were collected with an inexpensive apparatus (depicted schematically in Fig. 1) that contains an infrared LED operating at 890 nm and a silicon p–i–n photodiode.[1] The source was placed at a fixed central position on one side of the flask. On the other side, the detector was mounted upon a translation stage and moved to 25 locations at intervals of 0.2 cm (±2.4 cm). Magnitude and phase data were collected in the range of 10–81 MHz by use of a RF network analyzer.

To investigate the possible benefits of using multiple modulation frequencies, we selected data acquired at 10, 46, and 81 MHz. At each frequency, the 25 measurements were increased to 50 by use of the symmetry of the problem to assume that the same data would result from the detectors and source switching sides. Inversions were performed with individual frequencies and also with the three frequencies simultaneously. In all inversions, the domain (including the extrapolated boundary region computed for a refractive index of 1.33) was discretized into 65 × 33 × 65 nodes, giving grid spacings of 1.4 × 1.1 × 1.4 mm. The values of μ_a, D, and γ were initialized to 10^{-5} cm^{-1}, 0.05 cm, and 1.0, respectively. For the prior density, we used $\sigma = 2.0$ cm^{-1} and $p = 2.0$. The optimization procedure described above, in which one iteration consists of an update of all unknowns, was run for 100 iterations.

Reconstructed images of the absorption coefficient are shown in Fig. 2 for the measurement ($z = 0$) plane. Figures 2(a)–2(c) show single-frequency reconstructions obtained with modulation frequencies of 10, 46, and 81 MHz, respectively. Figure 2(d) shows the reconstruction obtained with all three modulation

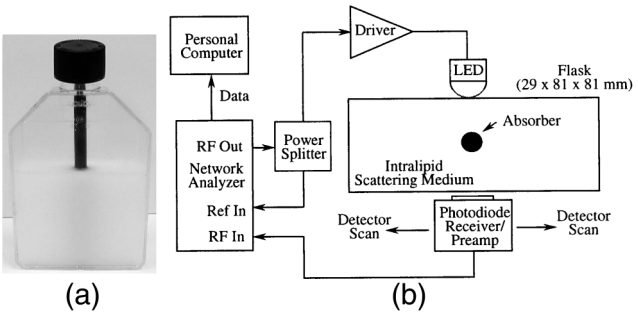

Fig. 1. (a) Culture flask with the absorbing cylinder embedded in a scattering Intralipid solution. (b) Apparatus used to collect the data.

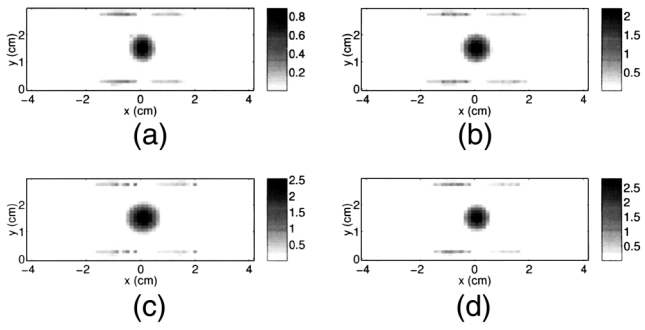

Fig. 2. Reconstructed images of the absorption coefficient with data at modulation frequencies of (a) 10, (b) 46, (c) 81, and (d) 10, 46, and 81 MHz.

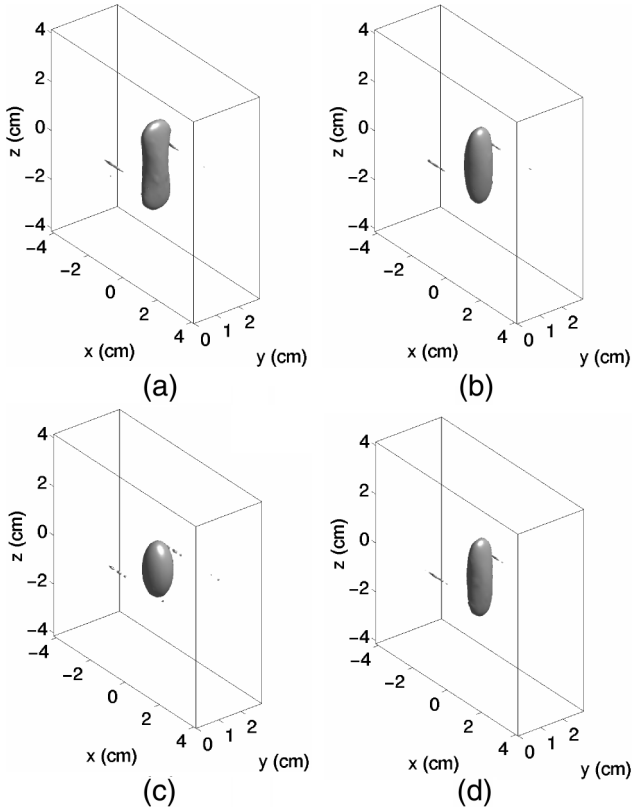

Fig. 3. Isosurfaces of the absorption coefficient images contoured at one quarter of the maximum value with data at (a) 10, (b) 46, (c) 81, and (d) 10, 46, and 81 MHz.

frequencies. All reconstructions show a circular, centrally located absorber of approximately the correct dimensions. Because the diffusion approximation does not apply in regions of high absorption, the actual values of the absorption within the cylinder cannot be quantitatively interpreted. Figure 3 shows isosurface plots of the absorption contoured at one quarter of the maximum value, corresponding to the reconstructions in Fig. 2. Despite the facts that data were collected only in a single plane and that no quasi-2-D assumptions were incorporated into the inversion geometry or into the prior model, the isosurfaces all resembled the cylindrical form of the absorber. The reconstruction in which all three modulation frequencies were used was slightly more accurate, suggesting that the use of multiple frequencies may offer advantages. All the reconstructions contain some artifacts in the vicinity of the detectors, possibly because of the slight asymmetry in the measured data, the failure of the diffusion approximation in the absorbing cylinder, or the influence of the Green's function singularity when the Fréchet derivative is evaluated near the detectors. The estimate of D was close to 0.08 cm, which is consistent with previous measurements,[1] except at 10 MHz, where it was somewhat lower. Using a single value of D (i.e., both outside and inside the absorbing cylinder) is not strictly correct and could introduce some error into the estimate.

In conclusion, we have presented a 3-D Bayesian inversion technique for optical diffusion absorption imaging and applied it to laboratory data. Estimation of source–detector coupling, background diffusion coefficient, and detector noise permit a fully automated reconstruction procedure. The results are geometrically accurate and show that the use of multiple modulation frequencies may be useful. They also demonstrate that use of a full 3-D model with Bayesian regularization allows 3-D images to be recovered from limited 2-D measurements. Accurate and efficient 3-D inversion methods such as this will be essential for practical optical diffusion imaging.

This research was supported by the National Science Foundation under contract CCR-0073357. K. J. Webb's e-mail address is webb@ecn.purdue.edu.

References

1. J. S. Reynolds, A. Przadka, S. Yeung, and K. J. Webb, Appl. Opt. **35,** 3671 (1996).
2. S. R. Arridge, Inverse Prob. **15,** R41 (1999).
3. J. C. Ye, K. J. Webb, C. A. Bouman, and R. P. Millane, J. Opt. Soc. Am. A **16,** 2400 (1999).
4. J. C. Ye, C. A. Bouman, K. J. Webb, and R. P. Millane, IEEE Trans. Image Process. **10,** 909 (2001).
5. F. E. W. Schmidt, J. C. Hebden, E. M. C. Hillman, M. E. Fry, M. Schweiger, H. Dehghani, D. T. Delpy, and S. R. Arridge, Appl. Opt. **39,** 3380 (2000).
6. N. Iftimia and H. Jiang, Appl. Opt. **39,** 5256 (2000).
7. F. Gao, P. Poulet, and Y. Yamada, Appl. Opt. **39,** 5898 (2000).
8. D. Boas, T. Gaudette, and S. Arridge, Opt. Express **8,** 263 (2001), http://www.opticsexpress.org.
9. R. C. Haskell, L. O. Svaasand, T.-T. Tsay, T.-C. Feng, M. S. McAdams, and B. J. Tromberg, J. Opt. Soc. Am. A **11,** 2727 (1994).
10. J. C. Ye, K. J. Webb, R. P. Millane, and T. J. Downar, J. Opt. Soc. Am. A **16,** 1814 (1999).